Simultaneous BOLD fMRI and fiber-optic calcium recording in rat neocortex

Kristina Schulz[1,2], Esther Sydekum[2,3,5], Roland Krueppel[1], Christoph J Engelbrecht[1,2,5], Felix Schlegel[2,3], Aileen Schröter[3], Markus Rudin[2–4] & Fritjof Helmchen[1,2]

Functional magnetic resonance imaging (fMRI) based on blood oxygen level–dependent (BOLD) contrast is widely used for probing brain activity, but its relationship to underlying neural activity remains elusive. Here, we combined fMRI with fiber-optic recordings of fluorescent calcium indicator signals to investigate this relationship in rat somatosensory cortex. Electrical forepaw stimulation (1–10 Hz) evoked fast calcium signals of neuronal origin that showed frequency-dependent adaptation. Additionally, slower calcium signals occurred in astrocyte networks, as verified by astrocyte-specific staining and two-photon microscopy. Without apparent glia activation, we could predict BOLD responses well from simultaneously recorded fiber-optic signals, assuming an impulse response function and taking into account neuronal adaptation. In cases with glia activation, we uncovered additional prolonged BOLD signal components. Our findings highlight the complexity of fMRI BOLD signals, involving both neuronal and glial activity. Combined fMRI and fiber-optic recordings should help to clarify cellular mechanisms underlying BOLD signals.

fMRI enables noninvasive monitoring of activity in healthy and diseased brains with submillimeter spatial resolution, in both humans and animals[1,2]. Commonly, alterations in BOLD contrast are used to estimate brain activity. However, BOLD measurements are indirect, as they arise from changes in cerebral blood flow, blood volume and oxygenation[3,4]. Understanding the link between BOLD signals and underlying neural activity is mandatory for interpreting fMRI results, particularly when studying pathological states with compromised neurovascular coupling[5]. Therefore, ideally, BOLD signals and neural activity are recorded simultaneously.

Simultaneous electrophysiological recordings in the MRI scanner have shown that local field potentials provide better estimates of cerebral blood flow and BOLD changes than multi- or single-unit activity[6]. However, electromagnetic interference compensation is technically challenging with this approach[6], and several key questions may be difficult to address, especially how specific neuronal or glial cell types connect to BOLD signals[7]. Hence, alternative methods to read out neuronal and glial activity in a simple, flexible and MRI-compatible way are desirable. Optical recording with an activity-dependent fluorescent indicator is such an alternative. Calcium indicators are suitable as they can probe various aspects of cortical dynamics *in vivo*, including neuronal network activation[8] and glial and metabolic signaling[9]. After loading of specific brain regions with calcium indicator[10], fluorescence signals can be recorded in a bulk fashion using single-photon excitation through an inexpensive optical fiber[11]. The MRI compatibility of optical fibers has been recently used to combine optogenetics and fMRI[12,13].

In this study, we combined BOLD fMRI with simultaneous fluorescence recording of neuronal and glial activity through an optical fiber. We determined how fiber-optically recorded calcium signals relate to BOLD signals in rat primary somatosensory cortex (S1) upon paw stimulation[14,15]. We applied a hemodynamic impulse response function to reconstruct BOLD signals from optically recorded neuronal responses that exhibit frequency-dependent adaptation. Furthermore, we describe additional BOLD signal components related to astrocytic network activity. Our hybrid approach directly links BOLD contrast to optically recorded activity in various brain cell populations and offers opportunities for future studies on neurovascular coupling in health and disease.

RESULTS

Combined setup for fMRI and fiber-optic calcium recording

We combined a fiber-optic fluorescence setup with a small-animal MRI scanner for simultaneously measuring neocortical activity with fluorescent calcium indicator and fMRI (**Fig. 1a**,**b** and Online Methods). After bulk labeling S1 with Oregon Green BAPTA-1 (OGB-1), we positioned the fiber tip above the forelimb region to elicit maximum fluorescence changes upon electrical forepaw stimulation. To prevent tissue damage, we avoided contact with the cortical surface. We secured the fiber tip in place using a cover plate and dental acrylic (**Fig. 1c**). In magnetic resonance images, the fiber tip appeared as a signal-void region in the agar above the craniotomy without any magnetic resonance image distortions (**Fig. 1d**). We avoided air-filled pockets known to cause image distortions by replenishing solution.

[1]Department of Neurophysiology, Brain Research Institute, University of Zurich, Zurich, Switzerland. [2]Neuroscience Center Zurich, University of Zurich and Swiss Federal Institute of Technology (ETH) Zurich, Zurich, Switzerland. [3]Institute for Biomedical Engineering, University of Zurich and ETH Zurich, Zurich, Switzerland. [4]Institute of Pharmacology and Toxicology, University of Zurich, Zurich, Switzerland. [5]Present addresses: Novartis Pharma Schweiz, Bern, Switzerland (E.S.) and E. Blum & Co. Ltd., Patent and Trademark Attorneys, Zurich, Switzerland (C.J.E.). Correspondence should be addressed to F.H. (helmchen@hifo.uzh.ch).

RECEIVED 8 APRIL 2011; ACCEPTED 28 MARCH 2012; PUBLISHED ONLINE 6 MAY 2012; DOI:10.1038/NMETH.2013

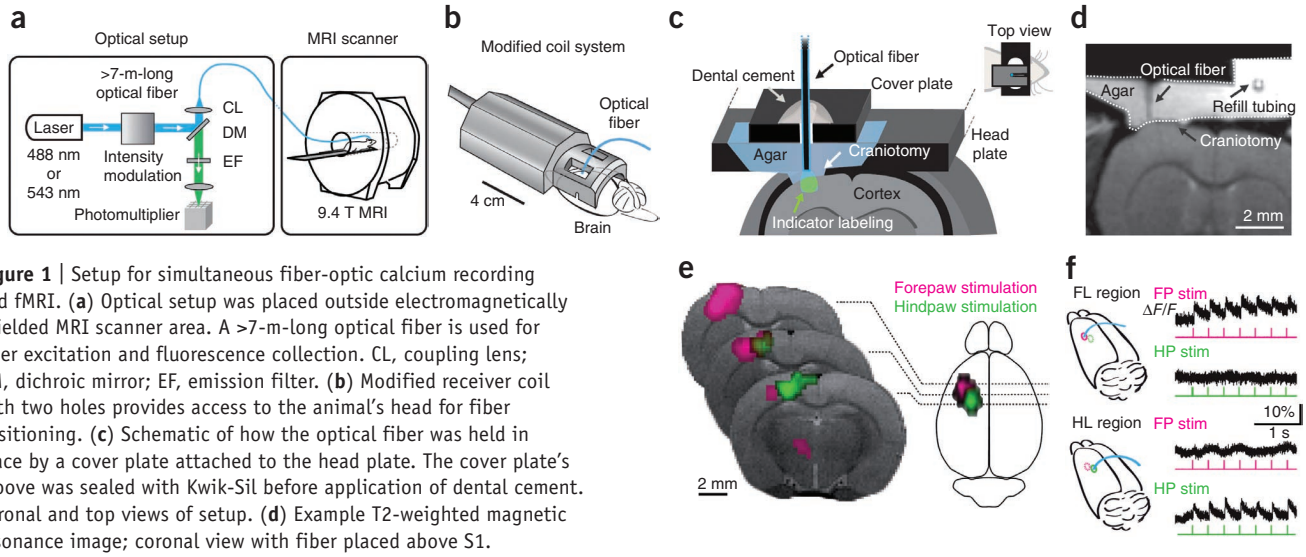

Figure 1 | Setup for simultaneous fiber-optic calcium recording and fMRI. (**a**) Optical setup was placed outside electromagnetically shielded MRI scanner area. A >7-m-long optical fiber is used for laser excitation and fluorescence collection. CL, coupling lens; DM, dichroic mirror; EF, emission filter. (**b**) Modified receiver coil with two holes provides access to the animal's head for fiber positioning. (**c**) Schematic of how the optical fiber was held in place by a cover plate attached to the head plate. The cover plate's groove was sealed with Kwik-Sil before application of dental cement. Coronal and top views of setup. (**d**) Example T2-weighted magnetic resonance image; coronal view with fiber placed above S1. Dotted outline, volume filled with agar and Ringer solution. Cross-section of thin tubing for refilling solution is indicated. (**e**) BOLD activation maps in three coronal sections in response to forepaw (magenta) and hindpaw (green) stimulation, respectively (all voxels with corrected $P < 0.01$). (**f**) Regionally localized fiber-optic fast OGB-1 calcium signals. Fiber was placed either above forelimb (FL) or hindlimb (HL) region and calcium signals were measured upon forepaw (FP) and hindpaw (HP) stimulation (stim).

Stimulation of either the forepaw or hindpaw with trains of brief electrical pulses activated neighboring regions in fMRI images consistent with S1 topography[14] (**Fig. 1e** and Online Methods). Similarly, in separate fiber-optic calcium measurements outside the MRI scanner, forepaw stimulation elicited fast fluorescence transients only when the fiber tip was positioned above the forelimb, but not the hindlimb, region, and vice versa for hindlimb stimulation (**Fig. 1f**). We conclude that both fMRI and fiber-optic calcium measurements show regionally confined activation in S1 upon paw stimulation.

Simultaneous fMRI and fiber-optic calcium recording

We next carried out simultaneous fMRI BOLD measurements and fiber-optic calcium recordings of OGB-1-labeled S1 using a block design stimulation paradigm ($n = 9$ rats; Online Methods). Five consecutive 3-Hz stimulation cycles caused BOLD responses and concomitant fiber-optic calcium signals, with significantly activated voxels located beneath the fiber tip (**Fig. 2a**,**b**). To evaluate the frequency dependence of responses and potential effects of neural adaptation, we systematically tested stimulations at 1 Hz, 3 Hz, 5 Hz and 10 Hz (**Fig. 2c**). BOLD signals showed similar onset times of 1–2 s for all frequencies. Mean amplitudes increased with frequency, showing saturation at 5–10 Hz (1 Hz, 1.8 ± 0.2%, $n = 9$; 3 Hz, 3.6 ± 0.3%, $n = 9$; 5 Hz, 4.4 ± 0.6%, $n = 8$; 10 Hz, 4.7 ± 1.2%, $n = 4$; all data are mean ± s.e.m.). Control measurements confirmed that direct irradiation of the cortex with laser light (<1 mW) affected neither the static MRI signal intensity ($n = 3$; $P = 0.30$, paired t-test) nor the evoked BOLD signal amplitude ($n = 5$; $P = 0.38$, repeated measures ANOVA; data not shown).

In the concurrent fiber-optic fluorescence recordings, individual stimuli evoked calcium transients with a fast rise followed by an exponential decay (**Fig. 2d**). Mean $\Delta F/F$ amplitude of the first transient during the first cycle was ~10%, independent of stimulation frequency. For 1-Hz stimulation, we fitted the decay of the first fluorescence transient with a single-exponential function, yielding a decay time constant of 0.16 ± 0.01 s ($n = 45$). At higher stimulation frequencies, interstimulus intervals were too short for transients to fully decay back to baseline, causing superposition of calcium transients. At the same time, neuronal responses adapted, with progressively lower $\Delta F/F$ amplitudes during the stimulus train. As a result of both superposition and adaptation, $\Delta F/F$ fluctuations typically reached a steady state during the stimulation period. To quantify adaptation we normalized $\Delta F/F$ amplitudes to the amplitude of the first response (**Fig. 2e**). At each stimulation frequency we found a significant reduction over time ($P < 0.001$; repeated measures ANOVA). The degree of adaptation was small for 1-Hz stimulation (74 ± 7% remaining $\Delta F/F$ amplitude in last 10 s of stimulation; $n = 9$ rats) and more pronounced at 3 Hz, 5 Hz and 10 Hz (remaining amplitudes: 40 ± 2%, $n = 9$; 23 ± 2%, $n = 8$; and 8 ± 4%, $n = 4$). Whereas adaptation with 1-Hz stimulation could be approximated with a single-exponential function (time constant 16.7 s), we observed a double-exponential decay at 3-Hz, 5-Hz and 10-Hz stimulation (fast time constants of 0.3 s, 0.1 s and 0.2 s; slow time constants of 29.6 s, 39.7 s and 67.5 s, respectively).

We conclude that our combined setup enables simultaneous measurements of fMRI BOLD signals and bulk calcium transients. To relate these two functional readouts in more detail, we next addressed two questions. First, what is the source of the fluorescence signals observed with bulk fiber-optic recording? And second, to what extent can we predict BOLD responses from the measured calcium transients?

Signal source in fiber-optic bulk calcium recordings

Fiber-optic recordings from labeled tissue report bulk fluorescence changes that depend on indicator type and labeling specificity. To examine the source of sensory-evoked OGB-1 signals, we did separate control experiments using *in vivo* two-photon calcium imaging[8]. OGB-1 nonspecifically stains neurons, glia and the surrounding neuropil, which contains a dense meshwork of axons, dendrites and glial cell processes[10]. Paw stimulation evoked variable responses in layer 2/3 neurons but robust and large calcium transients in the neuropil (**Fig. 3a**,**b**). When we analyzed the two-photon image series

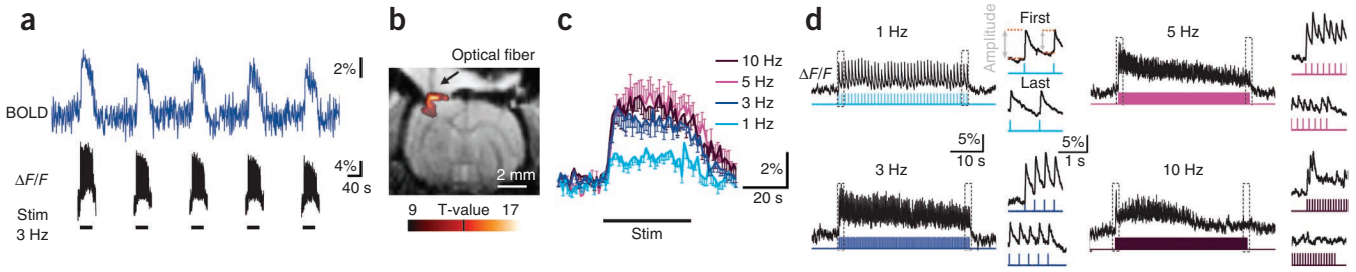

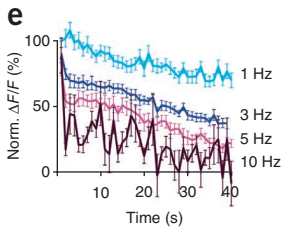

Figure 2 | Combined BOLD and fiber-optic measurements at various stimulation frequencies. (**a**) Example BOLD trace (blue) and simultaneously recorded bulk OGB-1 signal (black) in response to a block design forepaw stimulation (stim) at 3 Hz. On the compressed time scale, individual calcium transients are not discernible. (**b**) Coronal echo-planar imaging pulse scan through rat's head with significantly activated voxels ($P < 0.025$) overlaid. Fiber tip is visible as signal-void region (arrow). (**c**) BOLD signals in response to 40-s forepaw stimulation at different frequencies (1-Hz temporal resolution; $n = 5$ rats). Data are median ± s.e.m. (**d**) Example $\Delta F/F$ traces (smoothed with a 32-ms sliding average) in response to different stimulation frequencies. For each trace, first and last evoked responses are shown on expanded time scale. Calcium transient amplitude was calculated as difference between peak $\Delta F/F$ and prestimulus value (gray arrows). Mean ± s.e.m. $\Delta F/F$ amplitudes of first transients were 10.9 ± 0.2% (1 Hz; $n = 9$), 11.1 ± 1.8% (3 Hz; $n = 9$), 10.9 ± 0.8% (5 Hz; $n = 8$) and 10.6 ± 0.7% (10 Hz; $n = 4$; $P = 0.99$, ANOVA). (**e**) Adaptation of calcium signal amplitude (normalized to first stimulus response) at all stimulation frequencies (mean ± s.e.m.; binned in 1-s intervals).

at high temporal resolution, the neuropil calcium signals at various depths closely resembled the fiber-optic bulk calcium signals from the same cortical region (**Fig. 3c**). Because the fiber collects scattered fluorescence from a volume of a few hundred micrometers in diameter[11], these results indicate that under our experimental conditions fast fiber-optic signals predominantly report neuropil activation in superficial layers, most likely reflecting widespread activation of afferent axonal pathways and local dendrites rather than an average signal from only a small group of neurons[16].

During prolonged stimulation (10–40 s, as applied in fMRI experiments) fiber-optic OGB-1 recordings showed in some cases an additional slow component that was visible in the envelope curve of the repetitive fast calcium transients (**Fig. 3d**). To examine whether this second component might originate from sensory-evoked glia activation[17,18], we specifically stained the astrocytic network with the red calcium indicator Rhod-2 (ref. 19; **Fig. 3e**). Using two-photon imaging, we observed that paw stimulation induced initial increases in glial processes ('gliapil') that were sometimes, but not always, followed by delayed large waves of somatic activation, resembling the envelope signal in OGB-1 recordings (**Fig. 3f**). Similar to earlier reports[19–21], vertically running blood vessels in the field of view dilated with short latency and reached a steady-state diameter in response to paw stimulation (exponential fits, 1.6 ± 0.7 s delay; 7.8 ± 1.4 s onset time

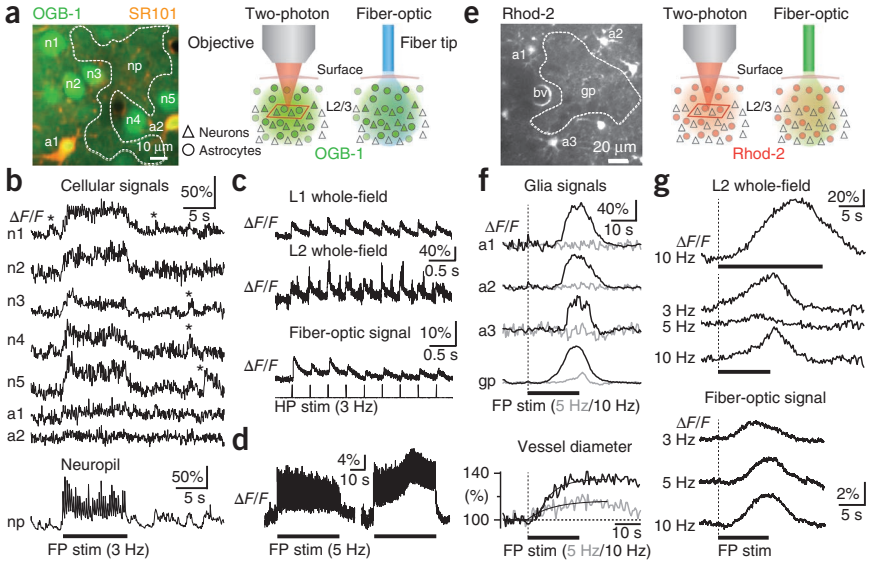

Figure 3 | Comparison of fiber-optic signals and two-photon calcium imaging data. (**a**) Left, two-photon image of OGB-1 labeled layer 2/3 cells in S1 forelimb region (neurons, green; sulforhodamine-101 counterstained astrocytes, orange). n, neurons; a, astrocytes; np, neuropil region. Right, schematic of mechanistic differences between two-photon microscopy and fiber-optic imaging. Two-photon microscopy provides cellular resolution (red box, imaged field of view) whereas optical fiber collects bulk volume signal. (**b**) Calcium transients in neurons (n1–n5), astrocytes (a1–a2), and np marked in **a** in response to 3-Hz forepaw stimulation. Asterisks, putative spontaneous neuronal calcium transients. (**c**) Comparison of neuropil OGB-1 calcium transients evoked by hindpaw stimulation in layers 1 and 2 of hindlimb region (20 µm and 100 µm, respectively, below pia) analyzed at high time resolution (Online Methods) with fiber-optic calcium transients collected from hindlimb region of same animal. (**d**) Two examples of fiber-optic OGB-1 recordings during 40-s forepaw stimulation with (right) and without (left) a distinct additional slow component. (**e**) Left, two-photon image of astrocytes specifically stained with Rhod-2. The blood vessel (bv) is surrounded by astrocytic endfeet. Regions devoid of somata contain labeled glial processes (gliapil, gp). Right, schematic of mode of action of two-photon microscopy and fiber-optic imaging with Rhod-2 bulk staining. Two-photon imaging records astrocytic signals with cellular resolution whereas fiber-optic signals represent astrocytic network activation. (**f**) Top, calcium transients in astrocytes (a1–a3) and gliapil (gp) marked in **e** in response to 5- and 10-Hz forepaw stimulation. Bottom, simultaneously recorded increases in blood vessel (bv) diameter fitted with exponential onsets. (**g**) Similarity of two-photon whole-field measurements of glial signals (top) and fiber-optical recordings from same cortical region (bottom).

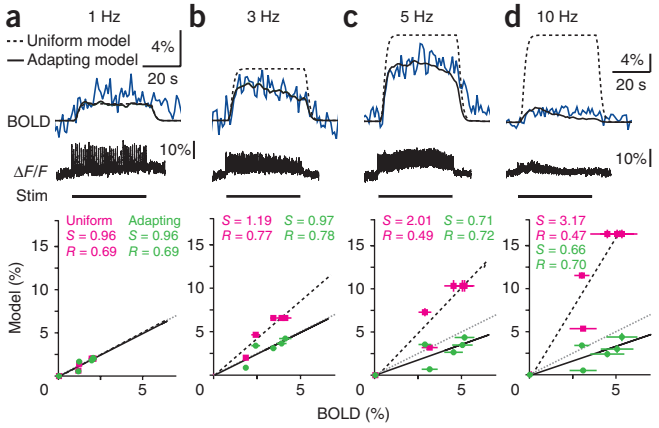

Figure 4 | Model reconstruction of BOLD changes from neuronal calcium responses. (**a**) Top, example of BOLD signal trace, model predictions and simultaneously recorded OGB-1 calcium trace evoked by 1-Hz forepaw stimulation. Uniform model (dashed line) assumes a uniform response to each stimulus, whereas adapting model (solid line) is generated from peak amplitudes of individual fluorescence traces evoked during stimulus train. Bottom, mean model amplitudes versus mean amplitudes of experimental BOLD signals (averages taken over seven 10-s segments around stimulation; mean ± s.e.m.). Linear fits to uniform model (interrupted line) and adapting model (solid line) as well as unity line (gray interrupted line). Values for slope *S* and correlation coefficient *R* are given. (**b**–**d**) Same analysis as in **a** for 3-Hz, 5-Hz and 10-Hz stimulation, respectively. Example traces, top; model versus actual BOLD plots, bottom. For both models correlations for all frequencies were highly significant ($P < 0.001$). Scale bars in **a** also refer to **b**,**c**.

constant; 24.8 ± 3.2% diameter increase at end of stimulation; $n = 9$). We could not determine the temporal order of vessel dilation and early gliapil calcium signals; however, the initial vascular response was independent of the large delayed glial activation because vessel dilation preceded this second component and also occurred in its absence (**Fig. 3f**; note lack of somatic astrocyte signals with 5-Hz stimulation, which nonetheless elicited gliapil and vascular responses).

Similar to OGB-1 results, two-photon–excited Rhod-2 fluorescence signals averaged over the whole field of view resembled fiber-optic signals measured from the same cortical region (**Fig. 3g**). Late glial calcium signals occurred with latencies of 4–20 s and had similar durations of 5–30 s for two-photon and fiber-optic measurements (full width at half maximum (FWHM), 15.9 ± 3.2 s, $n = 10$ and 14.6 ± 1.9 s, $n = 15$, respectively; $P = 0.71$, unpaired *t*-test). Although in some cases the onset was indicated by an inflection point, it was continuous in other cases, presumably because of asynchronous activation of the underlying astrocytic network. Bulk loading with Fluo-4, a different calcium indicator for astroglia-specific imaging[17], yielded similar two-photon imaging results (**Supplementary Fig. 1**; FWHM of 13.7 ± 2.1 s; 5–16 s latency; $n = 7$; $P > 0.7$). Fiber-optic $\Delta F/F$ amplitudes were smaller compared with two-photon wide-field measurements, presumably because of higher background signal. Incidence and amplitude of the delayed large glial calcium signals generally varied between trials but occurred preferentially at higher stimulation frequencies, longer durations and longer stimulation intervals (**Supplementary Fig. 1**). We conclude that prolonged paw stimulation can induce glial calcium signals with several components. The prominent delayed astrocytic network activation can be reliably detected with bulk fiber-optic recordings. Moreover, the glia-specific measurements confirm that the slow envelope components occasionally seen in OGB-1 recordings reflect additional glial activation on top of fast neuropil calcium transients.

Predicted BOLD signals from fiber-optic calcium recordings

We next examined to what extent BOLD changes can be predicted from fiber-optic OGB-1 recordings. We first disregarded stimulation cycles with evoked apparent glial responses. To translate neuronal activity into a vascular response, we assumed a hemodynamic impulse response function with time to peak of 2 s and FWHM of 2.5 s (ref. 22), which was summed in two ways to simulate BOLD changes. In the 'uniform model' each stimulus elicited a uniform response, neglecting adaptation. In the 'adapting model' the impulse responses were scaled according to the dynamically changing calcium transient amplitudes during stimulation, thus using the information regarding frequency-dependent adaptation (**Supplementary Fig. 2**). Uniform or scaled impulse responses were linearly summed and one proportionality factor relating calcium transient amplitude to BOLD response was determined for each rat (Online Methods).

To assess the ability of the two models to predict actual BOLD signals, we analyzed plots of modeled versus actual BOLD amplitude. For 1-Hz stimulation, both models predicted BOLD signals well (slope *S* close to unity), which did not surprise us given that little adaptation occurred (**Fig. 4a**). At higher stimulation frequencies the uniform model progressively overestimated the BOLD response amplitudes and the correlation coefficient *R* was lower (**Fig. 4b**–**d**), presumably because the plateau-like response shape did not capture the more variable BOLD time courses. The adapting model led to a better prediction of BOLD data, although it slightly underestimated amplitudes at higher frequencies. Using fiber-optic information on the temporal dynamics of neuronal responses, the correlation in this case remained high. In conclusion, we demonstrated a close link between fMRI BOLD changes and simultaneously recorded bulk calcium signals by accurately predicting BOLD signals from the adapting neuronal responses measured with the optical fiber.

Glia-related fMRI BOLD signal components

Finally, we investigated whether glia-related BOLD signal components might be detectable in trials with apparent large astrocytic activation. In three experiments we obtained fiber-optic Rhod-2 measurements of glial responses in the MRI scanner. In the example shown (**Fig. 5a**), the BOLD signal was prolonged in a trial with glia activation, as detected by Rhod-2, compared to a trial without glia signal. Subtracting the two BOLD responses showed the slow buildup of a glia-related BOLD component. Furthermore, we analyzed OGB-1 cycles with an additional slow envelope component as in **Figure 3d** ($n = 10$). These presumed glial events occurred more frequently in the first stimulation cycle ($n = 7$) and at high stimulation frequencies (incidence of 0%, 2%, 13% and 30% at 1 Hz, 3 Hz, 5 Hz and 10 Hz, respectively; $n = 45$, 45, 40 and 20, respectively). To uncover a potential glia-related BOLD component, we predicted the neuronal response component using the adapting model and subtracted it from the measured BOLD response (**Fig. 5b**). In cases with apparent glial activation the difference

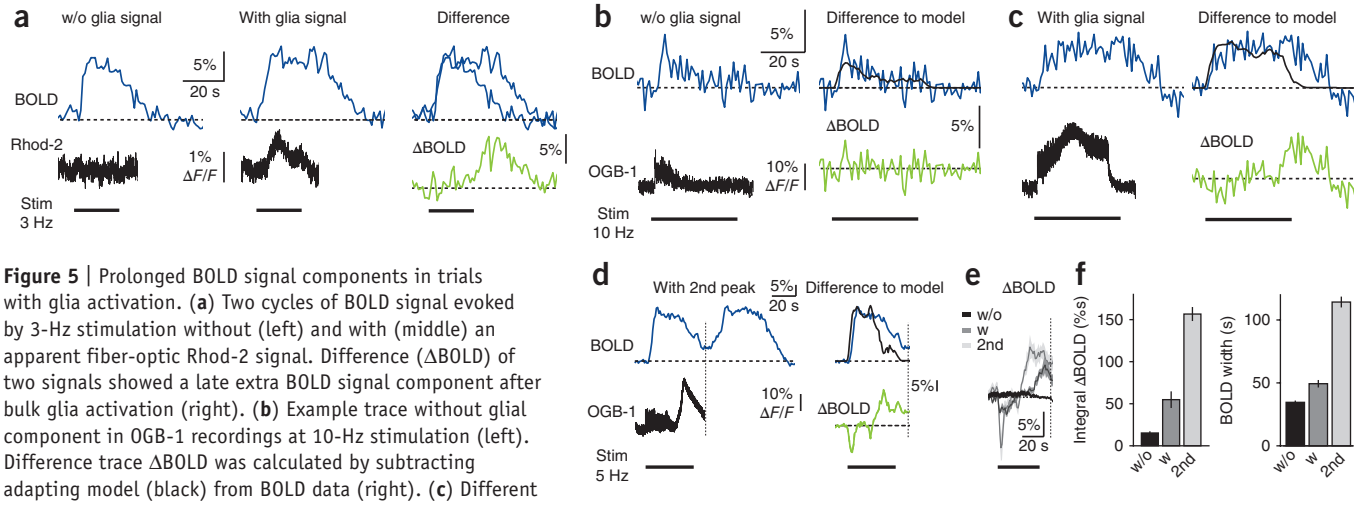

Figure 5 | Prolonged BOLD signal components in trials with glia activation. (**a**) Two cycles of BOLD signal evoked by 3-Hz stimulation without (left) and with (middle) an apparent fiber-optic Rhod-2 signal. Difference (ΔBOLD) of two signals showed a late extra BOLD signal component after bulk glia activation (right). (**b**) Example trace without glial component in OGB-1 recordings at 10-Hz stimulation (left). Difference trace ΔBOLD was calculated by subtracting adapting model (black) from BOLD data (right). (**c**) Different example from same animal with a clear slow component in OGB-1 signal (left). ΔBOLD trace calculated as in **b**. (**d**) 5-Hz stimulation example with a late secondary BOLD peak preceded by a large fiber-optic OGB-1 signal. ΔBOLD trace was calculated by subtracting adapting model estimate up to end of fluorescence recording 10 s after stimulation ceased (dashed line). (**e**) Average ΔBOLD signals for cycles without (w/o, $n = 80$, black) and with (w, $n = 6$, dark gray) glial component, and with late secondary BOLD peaks (2nd, $n = 4$, light gray; mean ± s.e.m.). (**f**) Integral of ΔBOLD traces (left; from stimulation onset to 10 s after stimulation) and BOLD signal widths (right) for the three respective groups.

trace (ΔBOLD) showed a late extra component, similarly to the Rhod-2 experiments, that was not present in trials lacking the slow additional envelope signal (**Fig. 5b**,**c**).

In four of the ten cases with apparent glial activation, we also observed a large secondary BOLD response that developed after the stimulation period (**Fig. 5d**; in three cases preceded by a very large OGB-1 signal). These double peaks occurred exclusively during the first cycle, mainly at high stimulation frequency (incidence in first cycle of 0%, 11%, 25% and 25% for 1 Hz, 3 Hz, 5 Hz and 10 Hz, respectively), and they showed widespread propagation throughout the hemisphere at a mean velocity of 4.9 ± 0.3 mm min^{-1} ($n = 4$; data not shown). Neuronal responses were transiently suppressed in the following stimulation cycles. On average, ΔBOLD traces for OGB-1 trials associated with a glial signal or a secondary BOLD peak contained an extra BOLD signal component compared to trials without such events (**Fig. 5e**). A quantitative analysis of the cumulative ΔBOLD trace integral and of the BOLD signal width showed significantly greater and longer BOLD changes in these cases (**Fig. 5f**; $P < 0.001$ ANOVA, $P < 0.05$ post-hoc Tukey-Kramer test for all comparisons). Our data demonstrate that under certain conditions BOLD fMRI signals can contain signal components beyond those that are well explained by neuronal activity.

DISCUSSION

The hybrid method for simultaneous recording of BOLD fMRI and bulk calcium indicator signals provides opportunities for directly linking BOLD responses to underlying neural activity. Combining electrophysiology with fMRI BOLD measurements to investigate this relationship is technically demanding owing to electromagnetic interference[6]. Our approach of combining optical recordings with fMRI is simple, inexpensive and straightforward as the optical setup can be placed sufficiently far from the MRI scanner and neither optical fibers nor laser-excited fluorescence signals interfere with fMRI. Furthermore, this approach offers flexibility and new potential applications that could facilitate further understanding of cellular mechanisms of neurovascular coupling. Here, we demonstrated such potential by linking neuronal and astrocytic calcium signals recorded from rat neocortex through an optical fiber to simultaneously measured BOLD signals.

Depending on indicator type, bulk calcium signals may reflect activity of various cellular compartments. For OGB-1 experiments, we concluded that fast fiber-optic calcium signals mainly reflect strong synaptic activation in the superficial cortical layers, on the basis of our two-photon imaging experiments and considering the pronounced attenuation of fluorescence collection with distance from the fiber tip[23]. Local field potential recordings, generally associated with synaptically driven dendritic activity, show frequency-dependent response characteristics similar to our results[15]. To link fiber-optic signals to BOLD fMRI, we simulated BOLD changes by convolving the stimulus train with a hemodynamic impulse response[22]. Our adapting model explicitly used temporal characteristics of adaptation shown by optical calcium recordings, accurately predicting BOLD responses for all stimulation frequencies and confirming the importance of neuronal adaptation for interpretation of BOLD signals[15].

Furthermore, we identified delayed slow calcium responses in OGB-1 recordings, and attributed these to stimulus-evoked astroglia activation. This interpretation was confirmed by additional experiments with astrocyte-specific staining using Rhod-2 and Fluo-4 (refs. 17,19). Astrocytic calcium signals have been implicated in sensory processing, brain metabolism and homeostasis, and disease states[7,9], but their exact function in neurovascular coupling remains debated[7]. We observed several distinct types of glial activation in response to sensory stimulation. Early calcium elevations in glial processes and endfeet (gliapil) may be related to metabotropic glutamate receptor signaling[7,24], although initiation of rapid hemodynamic responses does not depend on mGluR5 activation[25]. Because of the sensitivity and resolution of our measurements, however, we cannot make a firm conclusion about the chronology of gliapil signals and vascular response. As prominent delayed events during prolonged stimulations, we observed widespread concerted calcium elevations in astrocytic networks. These late events, which share features with reported

astrocytic signals[17,26], apparently occurred in an all-or-none fashion, perhaps triggered once a threshold for activation was surpassed. Although these glial responses did not initiate vessel dilations, they were associated with prolonged BOLD signals, suggesting a possible contribution to persistent vascular responses. A small undetected glial contribution to BOLD signals might also cause the slight underestimation of BOLD amplitude by the adapting model at higher stimulation frequencies (**Fig. 4**). Finally, rare large events in our fiber-optic recording, possibly comprising glial activation and neuronal depolarization shifts, were followed by late secondary BOLD signals that propagated throughout the cortical hemisphere. Their spatiotemporal characteristics and the transient subsequent suppression of neuronal responses match features of cortical spreading depression[7,27]. Concurrent fiber-optic and fMRI measurements may help clarify the nature and temporal order of the distinct astrocytic activation types and their relationship to neuronal activity and vascular response.

The possibility of targeting and discriminating specific cell types offers further prospects for studying cellular mechanisms of hemodynamic responses. Genetically encoded calcium indicators enable long-term functional imaging[28] and are compatible with fiber-optic recordings[29]. Using transgenic techniques or viral constructs with specific promoters[28,29], indicator expression can be restricted to specific subclasses of cells, including astrocytes[30]. Simultaneous studies of distinct cell populations should be feasible using multicolor labeling with different fluorescent probes. Moreover, virtually any brain area is accessible with fiber optics[11,12]. Finally, the combination of optogenetics and fMRI[12,13] may be enhanced by additional functional readout through optical fibers. In conclusion, this method presents new opportunities for gaining insights into neurovascular coupling and brain function.

METHODS

Methods and any associated references are available in the online version of the paper.

Note: Supplementary information is available in the online version of the paper.

ACKNOWLEDGMENTS

We thank M. Thallmair and B. Weber for helpful comments on the manuscript. This work was supported by the National Competence Center in Research program Neural Plasticity and Repair (M.R. and F.H.), the EU Seventh Framework Programme (SPACEBRAIN, project 200873, F.H.), the Swiss SystemsX.ch initiative (Neurochoice project, F.H.) and the Swiss National Science Foundation (grant 126029, M.R.).

AUTHOR CONTRIBUTIONS

F.H. and M.R. designed the research. C.J.E. and R.K. developed the optical setup. K.S. and R.K. did two-photon imaging experiments. K.S., E.S., F.S. and A.S. carried out simultaneous measurements of fMRI BOLD and OGB-1 fiber-optic fluorescence signals. E.S. and K.S. analyzed these BOLD data. R.K., F.S. and F.H. performed Rhod-2 and Fluo-4 measurements and F.S. analyzed the BOLD data. K.S. analyzed fluorescence traces. K.S. and F.H. developed the simulation models and wrote the paper.

COMPETING FINANCIAL INTERESTS

The authors declare no competing financial interests.

Published online at http://www.nature.com/doifinder/10.1038/nmeth.2013. Reprints and permissions information is available online at http://www.nature.com/reprints/index.html.

1. Logothetis, N.K. What we can do and what we cannot do with fMRI. *Nature* **453**, 869–878 (2008).
2. Rudin, M. *Molecular Imaging: Basic Principles and Applications in Biomedical Research* (Imperial College Press, 2005).
3. Heeger, D.J. & Ress, D. What does fMRI tell us about neuronal activity? *Nat. Rev. Neurosci.* **3**, 142–151 (2002).
4. Stephan, K.E., Weiskopf, N., Drysdale, P.M., Robinson, P.A. & Friston, K.J. Comparing hemodynamic models with DCM. *Neuroimage* **38**, 387–401 (2007).
5. Stefanovic, B., Schwindt, W., Hoehn, M. & Silva, A.C. Functional uncoupling of hemodynamic from neuronal response by inhibition of neuronal nitric oxide synthase. *J. Cereb. Blood Flow Metab.* **27**, 741–754 (2007).
6. Logothetis, N.K., Pauls, J., Augath, M., Trinath, T. & Oeltermann, A. Neurophysiological investigation of the basis of the fMRI signal. *Nature* **412**, 150–157 (2001).
7. Attwell, D. *et al.* Glial and neuronal control of brain blood flow. *Nature* **468**, 232–243 (2010).
8. Grewe, B.F. & Helmchen, F. Optical probing of neuronal ensemble activity. *Curr. Opin. Neurobiol.* **19**, 520–529 (2009).
9. Nedergaard, M., Rodriguez, J.J. & Verkhratsky, A. Glial calcium and diseases of the nervous system. *Cell Calcium* **47**, 140–149 (2010).
10. Stosiek, C., Garaschuk, O., Holthoff, K. & Konnerth, A. *In vivo* two-photon calcium imaging of neuronal networks. *Proc. Natl. Acad. Sci. USA* **100**, 7319–7324 (2003).
11. Adelsberger, H., Garaschuk, O. & Konnerth, A. Cortical calcium waves in resting newborn mice. *Nat. Neurosci.* **8**, 988–990 (2005).
12. Lee, J.H. *et al.* Global and local fMRI signals driven by neurons defined optogenetically by type and wiring. *Nature* **465**, 788–792 (2010).
13. Desai, M. *et al.* Mapping brain networks in awake mice using combined optical neural control and fMRI. *J. Neurophysiol.* **105**, 1393–1405 (2011).
14. Sydekum, E. *et al.* Functional reorganization in rat somatosensory cortex assessed by fMRI: elastic image registration based on structural landmarks in fMRI images and application to spinal cord injured rats. *Neuroimage* **44**, 1345–1354 (2009).
15. Kim, T., Masamoto, K., Fukuda, M., Vazquez, A. & Kim, S.G. Frequency-dependent neural activity, CBF, and BOLD fMRI to somatosensory stimuli in isoflurane-anesthetized rats. *Neuroimage* **52**, 224–233 (2010).
16. Kerr, J.N., Greenberg, D. & Helmchen, F. Imaging input and output of neocortical networks *in vivo*. *Proc. Natl. Acad. Sci. USA* **102**, 14063–14068 (2005).
17. Wang, X. *et al.* Astrocytic Ca^{2+} signaling evoked by sensory stimulation *in vivo*. *Nat. Neurosci.* **9**, 816–823 (2006).
18. Winship, I.R., Plaa, N. & Murphy, T.H. Rapid astrocyte calcium signals correlate with neuronal activity and onset of the hemodynamic response *in vivo*. *J. Neurosci.* **27**, 6268–6272 (2007).
19. Takano, T. *et al.* Astrocyte-mediated control of cerebral blood flow. *Nat. Neurosci.* **9**, 260–267 (2006).
20. Drew, P.J., Shih, A.Y. & Kleinfeld, D. Fluctuating and sensory-induced vasodynamics in rodent cortex extend arteriole capacity. *Proc. Natl. Acad. Sci. USA* **108**, 8473–8478 (2011).
21. Shen, Z., Lu, Z., Chhatbar, P.Y., O'Herron, P. & Kara, P. An artery-specific fluorescent dye for studying neurovascular coupling. *Nat. Methods* **9**, 273–276 (2012).
22. Silva, A.C., Koretsky, A.P. & Duyn, J.H. Functional MRI impulse response for BOLD and CBV contrast in rat somatosensory cortex. *Magn. Reson. Med.* **57**, 1110–1118 (2007).
23. Engelbrecht, C.J., Göbel, W. & Helmchen, F. Enhanced fluorescence signal in nonlinear microscopy through supplementary fiber-optic light collection. *Opt Express* **17**, 6421–6435 (2009).
24. Carmignoto, G. & Gomez-Gonzalo, M. The contribution of astrocyte signalling to neurovascular coupling. *Brain Res. Rev.* **63**, 138–148 (2010).
25. Calcinaghi, N. *et al.* Metabotropic glutamate receptor mGluR5 is not involved in the early hemodynamic response. *J. Cereb. Blood Flow Metab.* **31**, e1–e10 (2011).
26. Schummers, J., Yu, H. & Sur, M. Tuned responses of astrocytes and their influence on hemodynamic signals in the visual cortex. *Science* **320**, 1638–1643 (2008).
27. Dreier, J.P. The role of spreading depression, spreading depolarization and spreading ischemia in neurological disease. *Nat. Med.* **17**, 439–447 (2011).
28. Tian, L. *et al.* Imaging neural activity in worms, flies and mice with improved GCaMP calcium indicators. *Nat. Methods* **6**, 875–881 (2009).
29. Lütcke, H. *et al.* Optical recording of neuronal activity with a genetically encoded calcium indicator in anesthetized and freely moving mice. *Front Neural Circuits* **4**, 9 (2010).
30. Atkin, S.D. *et al.* Transgenic mice expressing a cameleon fluorescent Ca^{2+} indicator in astrocytes and Schwann cells allow study of glial cell Ca^{2+} signals *in situ* and *in vivo*. *J. Neurosci. Methods* **181**, 212–226 (2009).

ONLINE METHODS

Animal preparation. All experimental procedures were approved by the Veterinary Office of the Canton of Zurich and done in accordance with its guidelines. Female Lewis rats (~150 g, $n = 12$) were used for simultaneous fMRI and calcium recordings. Animals were housed in groups of three in standardized cages (Marcolon type IV) at a 12 h–12 h light-dark cycle with food and water *ad libitum*. They were given at least 1 week to acclimatize to their housing before experimentation. During surgery, rats were artificially ventilated with 3% isoflurane and the painkiller Rimadyl (5 mg per kg body weight) was delivered subcutaneously ($n = 8$). Four rats were prepared under 1.5% isoflurane and urethane (0.6 g per kg body weight) anesthesia and artificial ventilation was started when rats entered the MRI scanner. Depth of anesthesia was assessed by testing hindpaw withdrawal reflex. Rats were placed in a stereotactic frame in which the body temperature was maintained at ~37 °C with a warm-water heating system. The scalp was removed and a custom Plexiglas head-plate with an opening above the left S1 was fixed to the cleaned and dried skull using dental cement. A craniotomy (2 mm × 2.5 mm) was prepared over the forelimb region (Bregma coordinates, 3–5 mm, mediolateral; −1 to −1.5 mm, anterior-posterior). The dura was removed over a small restricted area within the craniotomy to avoid edema of brain tissue, which is more prominent in large exposed areas. Loading of the calcium-sensitive fluorescent dye OGB-1 (Invitrogen) was done according to the 'multicell bolus loading' protocol[10,31]. Briefly, 50 µg of the acetoxymethyl (AM) ester form of the calcium indicator was dissolved in 4 µl DMSO plus 20% (wt/vol) Pluronic F-127 (BASF) and then diluted with 36 µl standard pipette solution (150 mM NaCl, 2.5 mM KCl, 10 mM HEPES, pH 7.2), yielding a final OGB-1 concentration of ~1 mM. The dye was pressure ejected under visual control at two to four sites within the craniotomy in superficial layers using a glass pipette with broken tip. In acetoxymethyl-ester form, OGB-1 is membrane permeable and therefore loads neurons and astrocytes before becoming trapped inside the cells upon cleavage of the ester group. Preferential staining of astrocytes was done with Rhod-2 and Fluo-4 (Invitrogen; 50 µg acetoxymethyl-ester dye dissolved in 6 µl DMSO plus 20% (wt/vol) Pluronic F-127, diluted in 54 µl standard pipette solution). Solution (60 µl) was topically applied onto the exposed brain surface for at least 60 min, followed by thorough washing.

During MRI measurements animals were artificially ventilated with an air-oxygen mixture (80%/20%) and secured with ear bars on a cradle. Anesthesia during measurement blocks was continued with 1.1% isoflurane. The muscle relaxant gallamine (15 mg kg^{-1}; Sigma-Aldrich) was used to facilitate ventilation and prevent motion artifacts. Temperature was controlled with an MRI–compatible rectal probe and maintained at 36–37 °C with warm air flow or a warm-water heating system. Carbon dioxide partial pressure, p_{CO_2}, was monitored in a subset of animals using a transcutaneous electrode attached to the rat's thigh (TCM4, Radiometer). At the end of the experiment animals were killed with an overdose of pentobarbital (Sigma-Aldrich).

Setup for simultaneous fMRI and fiber-optic calcium recording. We used a standard animal MRI setup. Functional MRI data were collected in cross-coil mode using a whole-body resonator for radio-frequency transmission and a surface coil for signal reception operating at 400.3 MHz. This provided space for the hybrid setup within a cylinder of 70-mm inner diameter. To stay within the specifications for minimal fiber bending radius (~20 mm) the animal cradle was adapted so that the animal could be placed in ventral position with the intra-aural line of the stereotactic fixation located 10 mm below the magnet axis. Two holes in the receiver surface coil enabled the passage of the optical fiber for correct placement above either hemisphere (**Fig. 1b**). An optical fiber of ≥7-m length was used to guide both the fluorescence excitation light and the emitted fluorescence light between the optical setup (see below) and the animal inside the fMRI scanner. Optical recording equipment, which might interfere with the fMRI data acquisition, was placed outside the shielded magnet room. The optical fiber was fed into the Faraday cage via a cylindrical wave guide with an appropriate cutoff frequency. The optical fiber was positioned under visual control above the forelimb region of rat S1 using a stereotactic holder. Care was taken to leave cortical tissue intact. Thus direct contact of the fiber tip with the cortical surface was avoided, leaving a gap between fiber tip and cortex of a few hundred micrometers. The position of the fiber was adjusted to yield maximum fluorescence signal intensity in response to electrical forepaw stimulation. The fiber was held in place by a cover plate that rested on the head plate. Agar stabilized the craniotomy and filled the room between brain and cover plate (**Fig. 1c**). Gelfoam and Kwik-Sil (World Precision Instruments) were used to tightly seal the gap around the fiber. Once they were correctly positioned, the fiber tip and the cover plate were secured in place using dental acrylic. The craniotomy was kept moist by agar and Ringer solution, which was regularly replenished through thin tubing placed medially.

MRI and fMRI procedures. MRI experiments were done on a Bruker Biospec 94/30 horizontal-bore small-animal MRI scanner system (9.4 T self-shielded magnet with 30 cm clear bore; BGA-12S gradient insert with 120 mm inner diameter; gradient strength 440 mT m^{-1}; minimum slew rate 3,400 Tm^{-1} s^{-1}; Bruker Biospin). A quadrature volume resonator was used for radio-frequency transmission and a modified rat head surface coil operated in quadrature mode for signal detection. Coronal anatomical reference images were recorded using multislice rapid acquisition with relaxation-enhancement spin-echo sequence with the following parameters: field of view = 32.6 mm × 28.0 mm; matrix dimension = 175 × 150 pixels; slice thickness = 1 mm; interslice distance = 1 mm; echo time = 25 ms; effective echo time = 50 ms; repetition time (TR) = 1,500 ms; acceleration factor = 4; number of averages = 2; number of repetitions (NR) = 1; acquisition time = 1 min 51 s. Seven adjacent sections were recorded to cover large parts of the rat forebrain. The anterior commissure was chosen as landmark for positioning slices for fMRI data acquisition. The position of the fiber could be inferred from the anatomical scans (**Fig. 1d**). Using identical spatial dimension as in the anatomical reference images, BOLD-fMRI was done using a multislice gradient-echo echo-planar-imaging sequence (field of view = 32.6 mm × 28 mm; matrix dimension = 128 × 64 pixels; slice thickness = 1 mm; interslice distance = 1 mm; echo time = 13.62 ms; spatial resolution = 0.25 mm × 0.44 mm; NR = 56, TR = 1,250 ms, number of averages = 8 and frame interval = 10 s for rats 1–4; and NR = 1,200, TR = 1,000 ms, number of averages = 1, frame interval = 1 s and acquisition time = 20 min

for rats 5–12, respectively. The Mapshim algorithm was used to reduce distortions in echo-planar imaging images[32].

Optical setup for fluorescence recording. Fiber optics provides many options for fluorescence recordings[33–35]. Here, we carried out calcium recordings through an optical fiber with a custom optical setup. Vertically polarized light from an optically pumped semiconductor laser (Coherent Sapphire, 488 nm) was intensity adjusted with a variable metallic neutral density filter wheel (NDC-50C-4M). Laser intensity was <1 mW measured at the fiber tip to prevent photodamage. The laser beam was deflected off a dichroic beam-splitting mirror (BS R488, reflection 471–491 nm, >94%; transmission 503–900 nm, >93%; AHF Analysentechnik) and coupled into a hard polymer–clad multimode fiber (Thorlabs; BFL48-200; NA = 0.48; 230 µm cladding diameter) via an FC/PC fiber port (PAF-X-5, Thorlabs). Fluorescence excitation occurred in the vicinity of the fiber tip inside the MRI scanner and the emitted fluorescence light was collected and guided back to the optical setup through the same fiber. Fluorescence light passed the dichroic mirror and an emission filter (Semrock Razoredge; 488 Long Pass, AHF Analysentechnik) and was focused by a tube lens (AC254-030-A1-ML, Thorlabs) onto a peltier-cooled high-gain silicon photomultiplier including an transimpedance amplifier (SPMMini3000X03A1, SensL). For Rhod-2 recordings, a 543-nm He-Ne laser was used in conjunction with a beam-splitting mirror BS580 (AHF Analysentechnik). The photodetector signal was amplified by a wide-band variable-gain voltage amplifier (AMP, DHPVA-200, Femto Messtechnik) and digitized at 16 bits and 10 kHz using a USB-based data acquisition device (NI USB-6211, National Instruments). Data acquisition and stimulation were controlled with software custom-written in the LabVIEW environment (National Instruments).

Stimulation protocol. Rats were placed on the MRI cradle with optical fiber positioned above the labeled forelimb region, and bulk fluorescence changes were simultaneously recorded during electrical paw stimulation. The contralateral forepaw or, for control measurements, hindpaw was stimulated using bipolar needle electrodes placed subcutaneously. Stimulation pulses (0.5-ms duration) were delivered by a stimulus isolator (A365, WPI; 4 mA amplitude at 1 Hz, 3 Hz, 5 Hz or 10 Hz for forepaw stimulation; 2.5-mA amplitude at 3 Hz for hindpaw stimulation). Digit flexion threshold was determined before the first application of gallamine. A repetitive block design was used with one 'measurement' comprising five cycles that each consisted of an on period of 40 s, during which stimulation pulses were applied, and an off period of 140 s ($n = 5$) and 60 s ($n = 4$), respectively. For the combined fMRI and glial calcium fluorescence measurements, the cycles comprised an on period of 20 s and an off period of 320 s. Laser excitation was switched off in between cycles to avoid photobleaching. The sequence of measurements with different stimulation frequencies was randomized between animals. Not all frequencies were applied to each animal; for example, the four rats studied at lower temporal resolution of BOLD measurement (0.1 Hz) were not stimulated with 10 Hz. Rhod-2 experiments were done at 3-Hz stimulation. Between subsequent measurements, animals rested for about 10–15 min. For all animals with combined fMRI and fluorescence measurements, we confirmed a topologically correct positioning of fiber above the forelimb region by the absence of calcium signals in response to hindpaw stimulation. In additional control measurements we tested for potential hemodynamic effects caused by laser light, first by running five cycles with laser excitation on but without paw stimulation ($n = 4$ animals) and second by comparing five-cycle measurements with and without the laser turned on ($n = 1$ animal).

Two-photon imaging. In separate control experiments we carried out two-photon imaging to estimate the cellular contribution to calcium bulk signals collected with optical fiber. Nine female Lewis rats (OGB-1, $n = 4$; Rhod-2, $n = 4$; Fluo-4, $n = 2$) and ten Long Evans rats (OGB-1, $n = 6$; Rhod-2, $n = 1$; Fluo-4, $n = 3$; all ~150 g body weight) were used, with no noticeable difference in fluorescence signals between the two strains. Anesthesia and surgery were carried out as described above and body temperature was kept at 37 °C using a rectal probe and a heating pad. A custom two-photon microscope was used with a Ti:Sapphire laser system (MaiTai HP, Spectra-Physics), a Pockels cell (model 350/80 with controller model 302RM, Conoptics) for laser intensity adjustment, galvanometric scan mirrors (model 6210; Cambridge Technology), and a 40× objective (LUMPlanFI/IR 40x/0.80W, Olympus). Excitation wavelength was 865 nm. For control recordings in the hindlimb area, the craniotomy was placed at 2 mm to 4 mm mediolateral and −0.5 mm to 2 mm anterior-posterior from Bregma. Either OGB-1 AM bolus loading was done with an additional brief (1–5 min) topical application of sulforhodamine 101 (Sigma) to the cortical surface to counterstain astrocytes[36], or astrocytes were specifically labeled using 60-min surface application of Rhod-2 AM or Fluo-4 AM[17,19]. Calcium signals with single-cell resolution were collected at imaging speeds of 4–15.6 Hz (line duration 1–1.5 ms; image resolution from 64 × 128 pixels to 256 × 256 pixels). Images were background subtracted and relative percentage fluorescence changes ($\Delta F/F$) were calculated with a custom ImageJ macro. In the time series of two-photon images, synchronous activation of the superficial cortical layers upon stimulation was visible as fast, step-like fluorescence increases.

In a subgroup of animals (OGB-1, $n = 3$; Rhod-2, $n = 4$) single-photon bulk fluorescence measurements using optical fiber were made in the same animals in which two-photon imaging was done. For a direct comparison of fiber-optic recordings to the imaging data obtained with the two-photon microscope, we did line-wise analysis of the imaging frames. To gather specific information on neuropil activation, we restricted analyzed line segments to regions devoid of cell somata (**Fig. 3a**,**c**). Using line-wise analysis we achieved an effective temporal resolution of 0.667–1 kHz from the two-photon imaging data, thus mimicking the single-photon bulk fiber-optic recordings with 1.25-kHz sampling rate.

Data analysis and statistics. Statistical analysis of fMRI time series was done using the general linear model approach (Biomap ver. 4 and 4.2; M. Rausch, Novartis Institute for Biomedical Research). Thresholds for considering activation were $P < 0.025$ and a minimum area of 5 voxels. Time series were extracted from all voxels fulfilling the statistical criterion. A drift correction was made by fitting a polynomial through baseline measurements and subtracting the fitted curve from the experimental data.

doi:10.1038/nmeth.2013

Control measurements without laser light were compared to regular 3-Hz forepaw stimulation using repeated measures ANOVA. As optical recordings were restricted to stimulation periods, we carried out control measurements with laser illumination switched on during on periods while no electrical paw stimulation was delivered. For analysis, we used voxels defined by activity under 3-Hz stimulation. On and off blocks were pooled across animals and a paired *t*-test was used for statistical testing.

Data from fiber-optic recordings were first corrected for bleaching by fitting an exponential function to the baseline epochs (515 s) before and after the stimulation block and subtracting the resulting fit trace from the entire recorded episode. The background signal was determined as signal measured with closed shutter, that is, no laser excitation. Relative percentage change of fluorescence ($\Delta F/F$) was calculated by dividing the background-corrected signal ($F - F_0$) by the baseline fluorescence (F_0). The amplitudes of the fluorescence signal in response to each stimulus were calculated as the difference in $\Delta F/F$ in a time window 16–32 ms after stimulus and in a 16-ms preresponse window. To evaluate adaptation, $\Delta F/F$ amplitudes were normalized to the amplitude evoked by the first stimulus of the train. Significance of time-dependent changes was tested for each stimulation frequency by repeated measures ANOVA. Vessel dilations were quantified in ImageJ by measuring the perimeter of ellipses manually adjusted to the inside of astroglia-ensheathed arterioles. The percentage change in perimeter relative to the prestimulation period was used to estimate the percentage change in vessel diameter. All data are mean ± s.e.m.

Simulating the BOLD response. We used two models to simulate the BOLD response evoked by our stimulation protocols. In both models we assumed a linear summation of a hemodynamic impulse response (*IR*) to each single electrical stimulus. The impulse response was modeled on the basis of earlier measurements[22] as a gamma-variate function

$$IR(t) = (t-t_0)^r \exp(-k(t-t_0)), \text{ with } IR(t) = 0 \text{ for } t<t_0 \quad (1)$$

$r = 1.25$, $k = 1.07\ s^{-1}$ and $t_0 = 0.84$ s, leading to a time to peak of 2 s and a FWHM of 2.5 s. The model BOLD signal evoked by the stimulus trains was then calculated as

$$\text{mBOLD} = \text{SF}\sum_{k=1}^{n} A_k IR(t-t_k) \quad (2)$$

where SF is a global scale factor, n is the total number of stimuli per train, A_k is the amplitude evoked by each stimulus k during the train, and t_k is the onset time of the k^{th} stimulus.

In the first uniform model, a uniform response amplitude was assumed, with A_k set equal to the mean of the calcium signal amplitude at 1-Hz stimulation of the respective rat. In the second model, the adapting model, we used the amplitude A_k of the calcium signal evoked by each stimulus k to measure the strength of the neuronal response. Each simulation included all stimulation cycles of the respective rat, excluding cycles with apparent glial activation. The simulated data were downsampled to the experimental time resolution. To obtain the global scale factor SF, the downsampled time series of the adapting model was amplitude scaled using a least-squares fit to the according BOLD data. This scale factor was also used for the uniform model. SF accounts for experimental conditions such as variations in efficiency of receiver coil coupling affecting BOLD amplitude, variability in position of optical fiber, and differences between animals in absorption and scattering properties of tissue affecting optical signal. Although SF thus might differ among individuals, it should be relatively constant for each rat during an imaging session. For statistical comparison, bivariate Pearson correlations were carried out between BOLD data and model traces for each frequency. Data was averaged over 10-s segments and analysis was carried out on a 10-s prestimulation period, the 40-s stimulation period and a 20-s post-stimulation period.

For BOLD data with apparent glial activation in the simultaneously recorded fiber-optical signal, the adapting model was used to estimate the neuronal response component in the BOLD signal. In this case, the adapting model was generated as described above and fitted to the according BOLD data, generating another SF than was used for all nonglial trials. To estimate the 'glial component' of the BOLD signal, we calculated the difference between the recorded BOLD data and the adapting model estimation (ΔBOLD). The integral of the ΔBOLD trace was calculated for the stimulation block and the following 10-s period, thus considering only the time for which we recorded simultaneous fiber-optic signal. The width of the BOLD signal was calculated as the duration for which BOLD signal was >2 s.d. of the preceding baseline period. Statistical comparison between the three groups (without glial component, with glial component, and with secondary peak) was done using ANOVA and post-hoc Tukey-Kramer test for group comparisons.

31. Garaschuk, O., Milos, R.I. & Konnerth, A. Targeted bulk-loading of fluorescent indicators for two-photon brain imaging *in vivo*. *Nat. Protoc.* **1**, 380–386 (2006).
32. Gruetter, R. Automatic, localized *in vivo* adjustment of all first- and second-order shim coils. *Magn. Reson. Med.* **29**, 804–811 (1993).
33. Flusberg, B.A. *et al.* Fiber-optic fluorescence imaging. *Nat. Methods* **2**, 941–950 (2005).
34. Engelbrecht, C.J., Johnston, R.S., Seibel, E.J. & Helmchen, F. Ultra-compact fiber-optic two-photon microscope for functional fluorescence imaging *in vivo*. *Opt. Express* **16**, 5556–5564 (2008).
35. Fu, L. & Gu, M. Fibre-optic nonlinear optical microscopy and endoscopy. *J. Microsc.* **226**, 195–206 (2007).
36. Nimmerjahn, A., Kirchhoff, F., Kerr, J.N. & Helmchen, F. Sulforhodamine 101 as a specific marker of astroglia in the neocortex *in vivo*. *Nat. Methods* **1**, 31–37 (2004).

Nature Methods

Simultaneous BOLD fMRI and fiber-optic calcium recording in rat neocortex

Kristina Schulz, Esther Sydekum, Roland Krueppel, Christoph J Engelbrecht, Felix Schlegel, Aileen Schröter, Markus Rudin & Fritjof Helmchen

Supplementary Figure 1	Properties of glial calcium signals in S1 evoked by forepaw stimulation
Supplementary Figure 2	Schematic of model simulations

Supplementary Figure 1

Properties of glial calcium signals in S1 evoked by forepaw stimulation

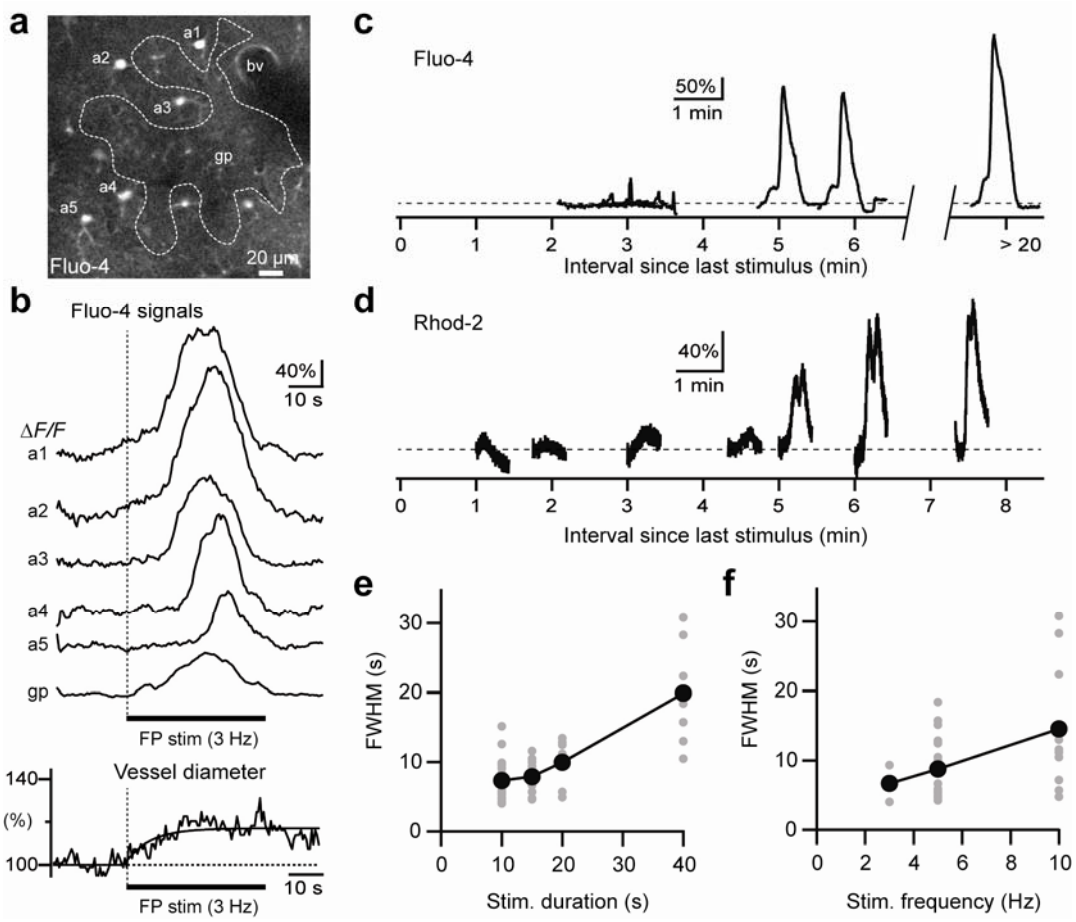

(**a**) Two-photon image of astrocyte-specific staining following surface application of the green fluorescent calcium indicator Fluo-4. Several astrocytes (a1-5), a cross-section of a blood vessel (bv), and a region for analysis 'gliapil' signal (gp) are indicated. (**b**) Fluo-4 calcium signals in 5 selected astrocytes and the gliapil evoked by 3 Hz forepaw stimulation for 40 s. Note the different onset times of somatic astrocyte signals. The corresponding percent increase in blood vessel perimeter for the vessel indicated in (a) is shown at the bottom together with an exponential onset fit. (**c**) Astrocytic calcium signals depended on the interval between stimulations. Fluo-4 signals upon 3-Hz forepaw stimulation for 40 s are shown as a function of the time interval elapsed since the previous stimulation cycle. Glia signals displayed a refractory period of a few minutes. (**d**) Same analysis as in (c) but for a Rhod-2 experiment with forepaw stimulation at 5 Hz for 20 s. Again Rhod-2 calcium signals required a few minutes to recover. (**e**) Dependence of FWHM of fiber-optically measured Rhod-2 calcium signals on duration of stimulation (3 Hz: n = 2, 5 Hz: n = 26, and 10 Hz: n = 10; data pooled). (**f**) Dependence of FWHM of fiber-optically measured Rhod-2 calcium signals on stimulation frequency (10-40 s stimulation durations pooled).

Supplementary Figure 2

Schematic of model simulations

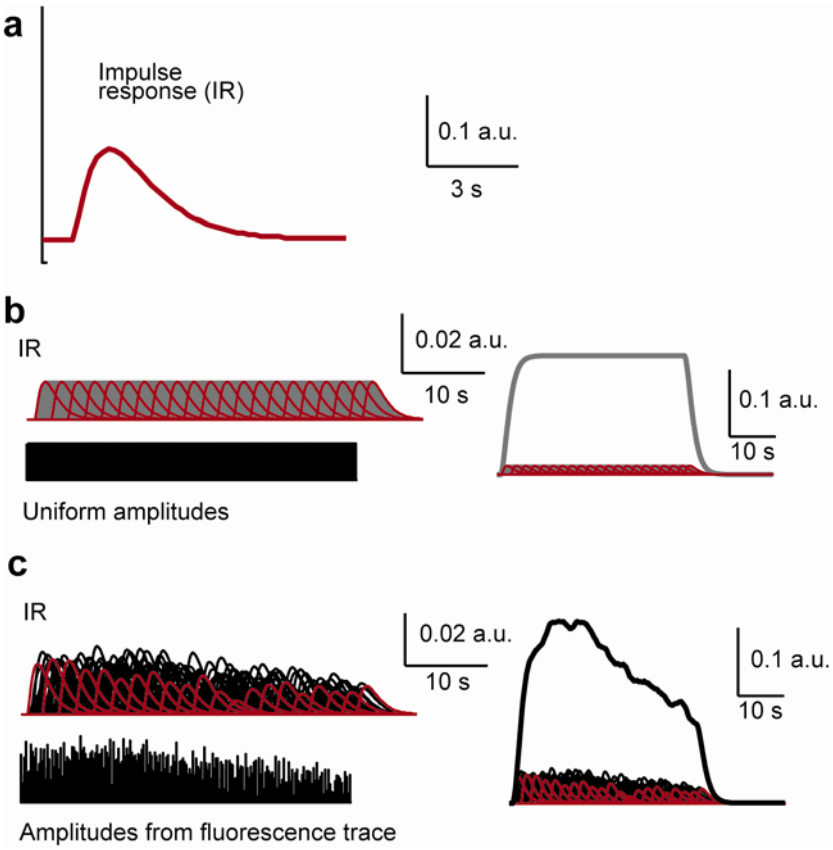

(**a**) Shape and timing of the assumed elementary hemodynamic impulse response (IR) function in response to a single stimulus. (**b**) Assuming a uniform response model each stimulus contributes the exact same IR (grey traces, every 10th trace highlighted in red). Summation of the IR train and down sampling in time to the acquisition rate of measured BOLD data (right). (**c**) Assuming adapting responses, each IR was scaled according to the measured fluorescence signal amplitude (black), generating a train of IR with variable amplitude which reflects the adaptation observed in the fiber-optic measurement. IR summation and down-sampling of simulated traces were performed as described in **b** (right). All blocks devoid of apparent glial component were taken into account to obtain the global scale factor for the respective experimental animal.